Journal of Organometallic Chemistry, 290 (1985) 199–211
Elsevier Sequoia S.A., Lausanne – Printed in The Netherlands

ELECTROCHEMISTRY AND X-RAY STRUCTURES OF THE ISOELECTRONIC CLUSTERS $[Fe_5C(CO)_{15}]$, $[N(PPh_3)_2][Fe_5N(CO)_{14}]$ AND $[NBu_4]_2[Fe_5C(CO)_{14}]$

ANDRÉ GOURDON and YVES JEANNIN*

Laboratoire de Chimie des Métaux de Transition, Université Pierre et Marie Curie, 4 Place Jussieu, 75230 Paris Cedex 05 (France)

(Received December 20th, 1984)

Summary

An electrochemical study and an X-ray investigation of isoelectronic $[Fe_5C(CO)_{15}]$, $[Fe_5N(CO)_{14}^-]$ and $[Fe_5C(CO)_{14}]^{2-}$ have been carried out. All three clusters are distorted square-based pyramids. The arrangement of CO ligands in each cluster is discussed. The displacement of the carbide (or nitride) atom from the basal mean plane increases with the cluster charge. The electrochemical reduction of $[Fe_5C(CO)_{15}]$ involves a two-electron transfer followed by loss of one CO ligand (slow at low temperatures) and leads to $[Fe_5C(CO)_{14}]^{2-}$.

Introduction

The strong interest in carbido and nitrido cluster chemistry stems from their structural similarities with surface carbides and nitrides believed to be intermediates in metal-catalysed hydrogenation reactions such as the Haber [1] and the Fisher–Tropsch [2] syntheses. Several theoretical [3], chemical [4–6], and spectroscopic studies [7–10] of square pyramidal clusters have been recently described *. We report here electrochemical and X-ray investigations of three isoelectronic carbide and nitride carbonyl clusters with different charges: $[Fe_5C(CO)_{15}]$, $[Fe_5N(CO)_{14}]^-$ and $[Fe_5C(CO)_{14}]^{2-}$.

Results

Electrochemistry

The single sweep cyclic voltammogram of a freshly prepared CH_2Cl_2 solution of

* For a comparison (geometry, spectroscopy and chemistry) between the pentanuclear family and the hexanuclear and tetranuclear analogues, see a recent review by J.S. Bradley [11] and references therein.

0022-328X/85/$03.30

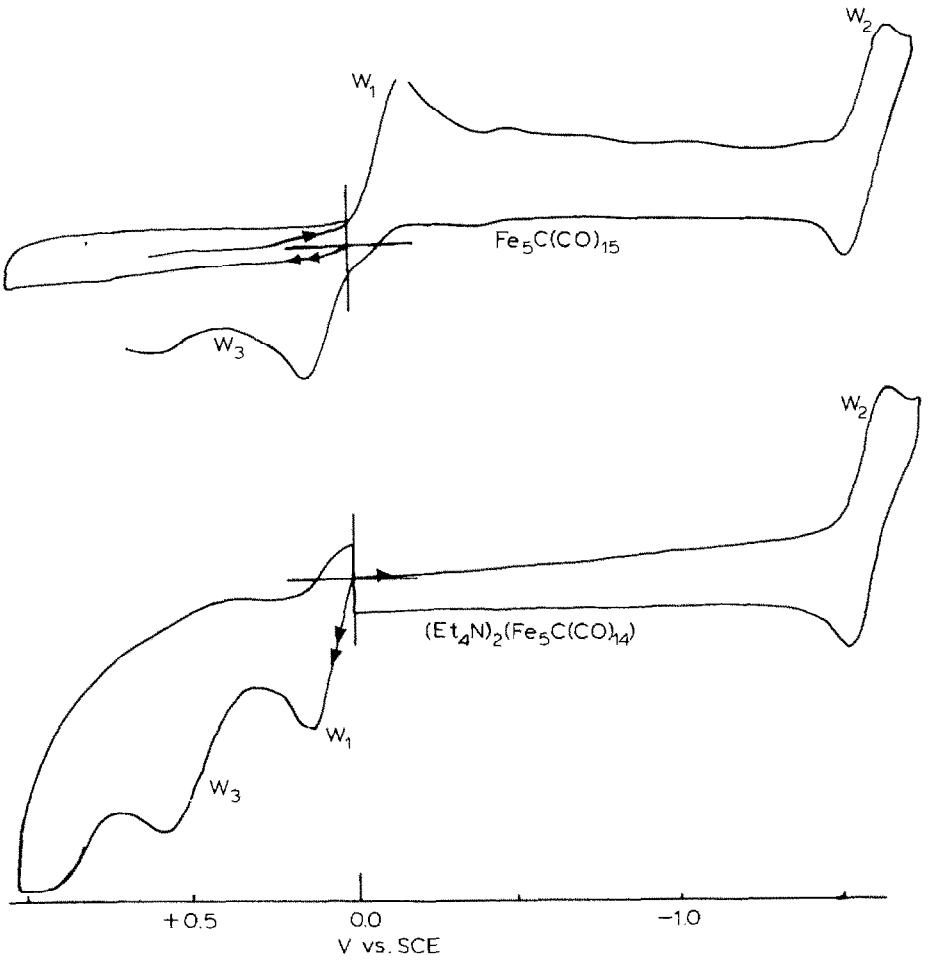

Fig. 1. Cyclic voltammograms of $[Fe_5C(CO)_{15}]$ and $[Et_4N]_2[Fe_5C(CO)_{14}]$ in CH_2Cl_2 at 20°C (vs. SCE, scan rate 100 mV s^{-1}).

$[Fe_5C(CO)_{15}]$ at 20°C is shown in Fig. 1. The first reduction wave W_1 is irreversible * [12]; a second wave W_2 appears at more negative potentials and looks quasi-reversible, with $E_{1/2}$ −1.58 V. The reverse scan shows an additional wave W_3 at 0.6 V vs. SCE. Figure 2 shows the first wave W_1 at various temperatures. Above 20°C the process is irreversible, with $E^{red}_{pW_1}$ −0.17 and $E^{ox}_{pW_1}$ +0.13 V vs. SCE. At lower temperatures, this latter reoxidation wave decreases as a new wave appears at −0.06 V. Below −15°C there is only one reoxidation wave, at −0.06 V, and the first reduction process appears quasi-reversible, with $E_{1/2}$ −0.115 V. If the scan is stopped for a few seconds at −0.40 V, the wave at +0.13 V reappears. $[Fe_5C(CO)_{15}]$ decomposes slowly in CH_2Cl_2 at room temperature; after a few hours, the cyclic voltammogram shows additional ill-defined waves between −1.0 and −1.5 V. When

* From comparisons with published results for similar compounds, systems showing peak separations up to 100–120 mV are considered quasi-reversible; $E_{1/2}$ is then defined as $(E^{red}_p + E^{ox}_p)/2$.

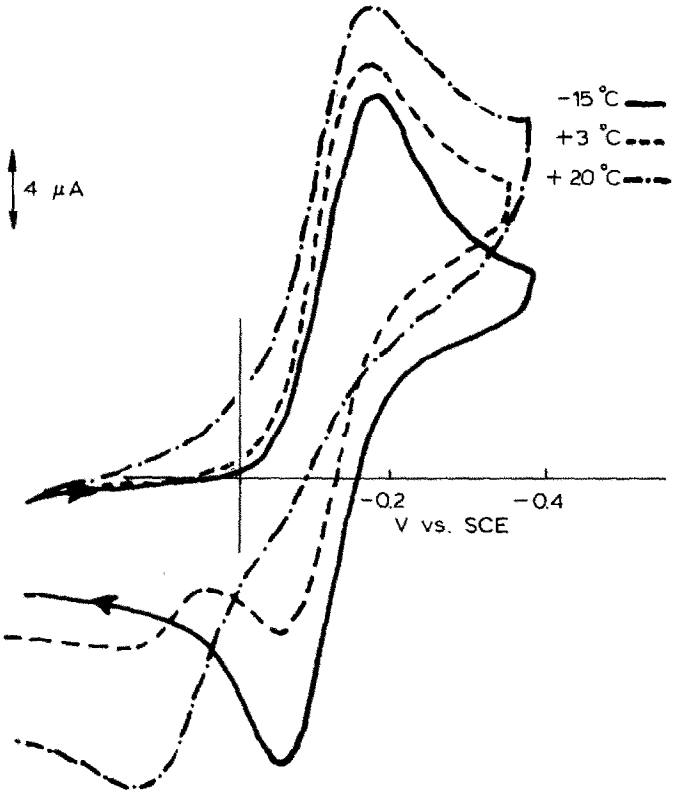

Fig. 2. Cyclic voltammograms of $[Fe_5C(CO)_{15}]$ at different temperatures.

this decomposition is taken into account, room temperature exhaustive reduction of $[Fe_5C(CO)_{15}]$ in CH_2Cl_2 at -0.6 V requires 2 F mol^{-1}; the reduction leads to $[Fe_5C(CO)_{14}]^{2-}$, as shown by infrared spectroscopy and cyclic voltammetry after electrolysis. The cyclic voltammogram of $[Et_4N]_2[Fe_5C(CO)_{14}]$ in CH_2Cl_2 at 20°C is shown in Fig. 1. It presents a set of waves W_1, W_2 and W_3 similar to those from $[Fe_5C(CO)_{15}]$ at 20°C.

These results can be interpreted as follows. The first electron process W_1 can be written as:

$$[Fe_5C(CO)_{15}] + 2e^- \overset{A}{\rightleftharpoons} [Fe_5C(CO)_{15}]^{2-} \overset{B}{\rightarrow} [Fe_5C(CO)_{14}]^{2-} + CO$$

Below -15°C the quasi-reversible wave is assigned to the $2e^-$ transfer A; the CO loss in reaction B is slow with respect to the scanning time at this temperature. At higher temperatures or when the scan is halted at -0.4 V, $[Fe_5C(CO)_{15}]^{2-}$ partially decomposes through B by loss of one CO and the wave at $+0.13$ V appears (oxidation of $[Fe_5C(CO)_{14}]^{2-}$). Above 20°C reaction B is fast. After the first $2e^-$ reduction, the cyclic voltammogram of $[Fe_5C(CO)_{15}]$ is that of $[Fe_5C(CO)_{14}]^{2-}$. Comparison of the peak heights of the other reduction waves of $[Fe_5C(CO)_{15}]$, $[Fe_5N(CO)_{14}]^-$ and $[Fe_5C(CO)_{14}]^{2-}$ with W_1 indicates that all these reductions are two-electron processes. Cyclic voltammetry data are given in Table 1.

TABLE 1

CYCLIC VOLTAMMETRY DATA[a]

Compound	First reduction and corresponding reoxidation		Second reduction and corresponding reoxidation		First oxidation		Further oxidation
	E_p^{red}	E_p^{ox}	E_p^{red}	E_p^{ox}	E_p^{ox}	E_p^{red}	
$Fe_5C(CO)_{15}$	−0.17	+0.13 +0.60	−1.63	−1.53	–	–	–
	(oxidation waves of $Fe_5C(CO)_{14}^{2-}$)		(first reduction of $Fe_5C(CO)_{14}^{2-}$)				
Below −15°C	−0.17	−0.06	−1.60	−1.50	–	–	–
$Fe_5C(CO)_{14}^{2-}$	−1.63	−1.53	–	–	0.12	0.02	0.6
$Fe_5N(CO)_{14}^{-}$	−1.30	−1.18	–	–	0.63	0.50	–

[a] In V vs. SCE. Solutions 10^{-3} *M* in CH_2Cl_2, 0.1 *M* Bu_4NBF_4. Carbon electrode, scan rate 100 mV s^{-1}. *T* 293 K if not specified.

X-ray structure analyses

Dahl and coworkers reported in 1962, the synthesis and the structure of the first carbido carbonyl cluster $[Fe_5C(CO)_{15}]$ [13]. From recrystallizations of this compound in CH_2Cl_2, we obtained two polymorphs with slightly different metal carbido infrared stretching frequencies in the solid state, namely needles (Dahl's structure), with bands at 805 and 765 cm^{-1}, and plates, with bands at 805 and 780 cm^{-1}. The

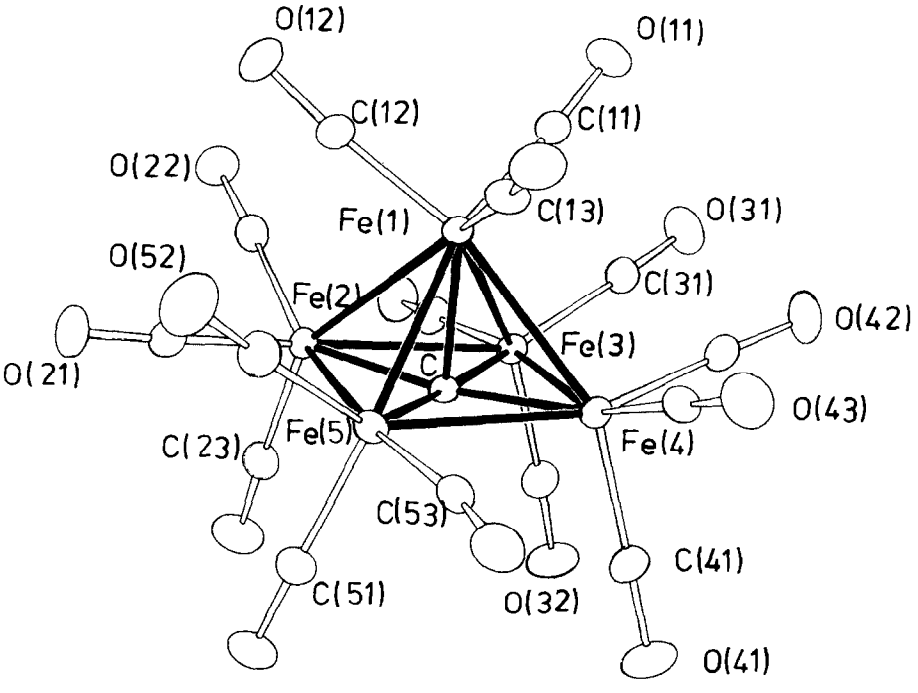

Fig. 3. A view of $[Fe_5C(CO)_{15}]$.

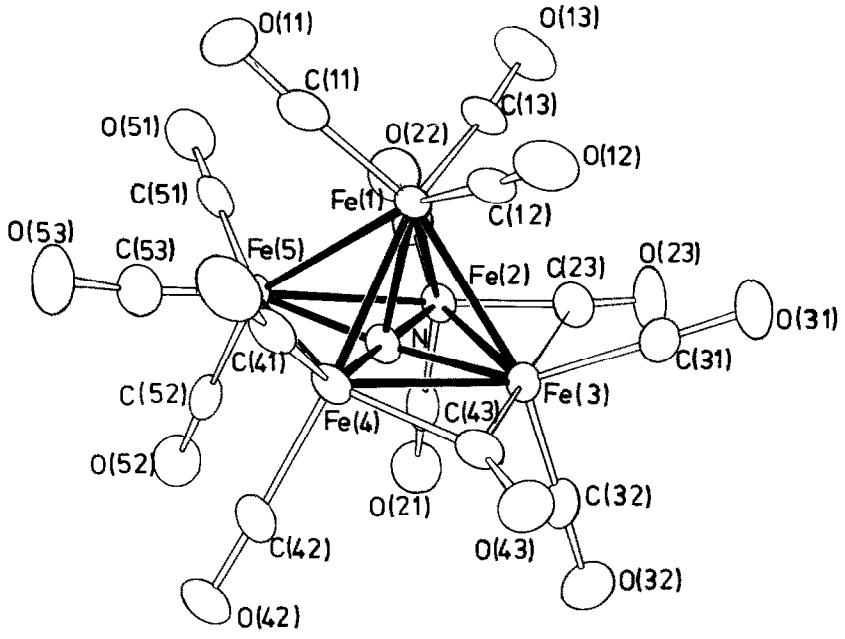

Fig. 4. A view of the anion $[Fe_5N(CO)_{14}]^-$.

infrared spectra recently reported by Oxton et al. [8] represent the superposition of these bands and in neither case did we observe crystal field splitting. The Ru and Os analogues [4,5] $[Ru_5C(CO)_{15}]$ and $[Os_5C(CO)_{15}]$ have the same type of complex IR spectra. The extra bands observed for these compounds result from the presence in the same unit cell of two non-equivalent sets of molecules. In order to determine the accurate geometry of this polymorph, we determined its structure by a single crystal X-ray study.

The structures of $[Fe_5C(CO)_{15}]$ (**1**), $[Fe_5N(CO)_{14}]^-$ (**2**) and $[Fe_5C(CO)_{14}]^{2-}$ (**3**) are shown in Figs. 3,4 and 5, together with the atom numbering schemes. The iron skeletons have a similar distorted square-based pyramid geometry. They are formally 74-electron systems and strictly follow Wade's rules [14]. The overall geometry of **1** is very similar to that described by Dahl and coworkers. The high *R* factor in Dahl's structure determination (resulting from visually estimated intensities of Weissenberg photographs) prevents detailed comparisons with **1**. In **1** the Fe–Fe distances show a surprisingly large spread of values from 2.714(2) to 2.615(2) Å. In the charged clusters, the Fe(apical)–Fe(basal) bond lengths are significantly shorter (mean 2.585(4) in **2**, 2.598(4) Å in **3**) than in the neutral cluster (mean 2.647(2) Å). There is no bond lengthening influence of the basal bridging CO group on these Fe(apical)–Fe(basal) bonds such as was observed in $[Os_5C(CO)_{14}]^{2-}$ [4]. In both of the anions **2** and **3** the basal Fe–Fe bonds associated with the bridging and semi-bridging carbonyl groups are ca.0.1 Å shorter than the non-bridged basal Fe–Fe bonds.

In $[Fe_5C(CO)_{15}]$ one of the three terminal CO groups of each basal Fe atom is roughly *trans* with respect to one Fe(basal)–Fe(basal) bond. These four carbonyl groups [(21), (33), (42) and (53)] interact with the adjacent basal Fe atom, as shown

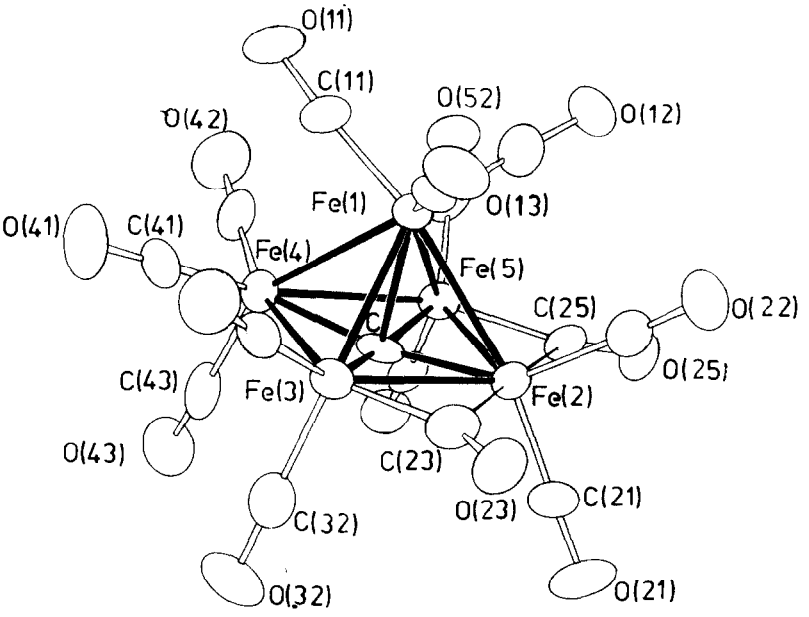

Fig. 5. A view of the dianion $[Fe_5C(CO)_{14}]^{2-}$.

by the fact that the Fe–C–O angles are significantly smaller [mean 171.4(6)°] than the other Fe(basal)–C–O angles [mean 176.9(10)°]. Although this semi-bridging interaction usually has a bond lengthening effect on the Fe–C bond length, these four Fe–C are actually shorter than the other Fe–C(carbonyl) bonds.

TABLE 2

CRYSTAL DATA AND REFINEMENT PARAMETERS FOR $[Fe_5C(CO)_{15}]$ (**1**), $[N(PPh_3)_2]$-$[Fe_5N(CO)_{14}]$ (**2**) AND $[NBu_4]_2[Fe_5C(CO)_{14}]$ (**3**)

	1	**2**	**3**
Formula	$C_{16}Fe_5O_{15}$	$C_{50}H_{30}Fe_5N_2O_{14}P_2$	$C_{47}H_{72}Fe_5N_2O_{14}$
M	711.40	1223.98	1168.33
Crystal system	Monoclinic	Monoclinic	Monoclinic
a (Å)	15.135(8)	17.48(1)	12.719(3)
b (Å)	9.234(6)	15.99(2)	24.56(2)
c (Å)	32.97(3)	22.23(2)	21.68(2)
β (°)	103.39(5)	123.93(4)	124.53(4)
U (Å^3)	4482(12)	5156(16)	5580(13)
Z	8	4	4
$F(000)$	1648	2464	2440
Space group	$C2/c$	$P2_1/c$	$P2_1/c$
μ(Mo-K_α cm^{-1})	32.64	14.95	13.26
2θ-limits	$3 < 2\theta < 48$	$3 < 2\theta < 40$	$3 < 2\theta < 40$
Reflections used in refinement	2870	2690	3058
Weighting scheme : $w = 1/\lvert\sigma(F)\rvert^2$			
$R = \Sigma\lvert(F_{obs} - F_{calc})\rvert/\Sigma F_{obs}$	0.044	0.052	0.071
$R_w = \{\Sigma w(F_{obs} - F_{cal})^2/\Sigma w(F_{obs})^2\}^{1/2}$	0.049	0.055	0.060

In the monoanion **2**, one carbonyl ligand bridges asymmetrically one of the Fe–Fe basal bonds (Fe(3)–C(43) 2.05(2), Fe(4)–C(43) 1.96(1) Å).

A small semi-bridging interaction between C(23)–O(23) and Fe(3) compensates for an imbalanced charge on Fe(3) (Fe(2)–C(23)–O(23) 164(2)°).

In the dianion **3**, two carbonyl ligands [(25) and (23)] are semi-bridging over two adjacent basal Fe–Fe bonds [Fe(5)–C(25) 1.85(2), Fe(3)–C(23) 1.82(2), and Fe(2)–C(25) 2.28(2), Fe(2)–C(23) 2.15(2) Å]. This geometry is consistent with the IR spectrum, which contains a bond at 1735 cm^{-1} characteristic of an edge-bridging CO.

The carbide (respectively nitride) atoms are located below the iron basal mean plane. The distance from this plane increases with cluster charge with values of 0.09(1) for **1**, 0.11(1) for **2** and 0.18(1) Å for **3**. It is noteworthy that the same feature can be observed in the analogous Ru clusters $[Ru_5C(CO)_{15}]$,$[Ru_5C(CO)_{14}(PPh_3)]$ and $[Ru_5C(CO)_{13}(PPh_3)_2]$ recently described by Lewis and coworkers [5]. In these compounds, the distance between the carbide atom and the Ru_4 mean plane increases with phosphine substitution from 0.11(2) to 0.23(1) Å. The replacement of a CO ligand by a less π-acidic phosphine similarly formally increases the negative charge of the cluster framework. These structural results are in good agreement with spectroscopic data for a series of carbido and nitrido ion clusters [7,10]. ^{57}Fe Mössbauer spectroscopy shows that the isomer shift increases from $[Fe_5C(CO)_{15}]$ to $[Fe_5N(CO)_{14}]^-$ and to $[Fe_5C(CO)_{14}]^{2-}$. According to Sosinsky and coworkers, this feature may indicate that the electron charge in the iron framework shifts to the carbido carbon atom when the anionic charge is increased. This electron localization could explain the corresponding observed distortion of the framework toward octahedral.

TABLE 3

SELECTED BOND LENGTHS (Å) AND ANGLES (°) FOR $[Fe_5C(CO)_{15}]$ (**1**)

Fe(1)–Fe(2)	2.615(2)	Fe(1)–C(11)	1.829(7)
Fe(1)–Fe(3)	2.714(2)	Fe(1)–C(12)	1.799(6)
Fe(1)–Fe(4)	2.624(1)	Fe(1)–C(13)	1.799(6)
Fe(1)–Fe(5)	2.636(2)	Fe(2)–C(21)	1.799(7)
Fe(2)–Fe(3)	2.650(2)	Fe(2)–C(22)	1.841(6)
Fe(2)–Fe(5)	2.671(1)	Fe(2)–C(23)	1.823(7)
Fe(3)–Fe(4)	2.683(1)	Fe(3)–C(31)	1.837(7)
Fe(4)–Fe(5)	2.682(2)	Fe(3)–C(32)	1.813(7)
		Fe(3)–C(33)	1.804(6)
Fe(1)–C	1.953(5)	Fe(4)–C(41)	1.816(7)
Fe(2)–C	1.903(4)	Fe(4)–C(42)	1.807(7)
Fe(3)–C	1.877(5)	Fe(4)–C(43)	1.820(6)
Fe(4)–C	1.911(5)	Fe(5)–C(51)	1.820(7)
Fe(5)–C	1.873(5)	Fe(5)–C(52)	1.819(7)
		Fe(5)–C(53)	1.793(6)
C–O 1.13–1.16			
max. e.s.d. 0.01			
mean 1.14			
Fe–C–O 170.0–179			
max. e.s.d. 1			
mean 174.8			

Experimental

Syntheses

All complexes were synthesized and handled under nitrogen or argon using dry distilled solvents. The compounds $[Fe_5C(CO)_{15}]$ and $[N(PPh_3)_2][Fe_5N(CO)_{14}]$ were prepared by published methods [15,16]. Crystals of the latter compound were obtained by slow cooling of a methanolic solution. $[NBu_4]_2[Fe_5C(CO)_{14}]$ was obtained by controlled-potential electrolysis of $[Fe_5C(CO)_{15}]$ in CH_2Cl_2 at room temperature at -0.6 V vs. SCE. The solvent was then evaporated under vacuum. The brown precipitate was washed with water, dried under vacuum, and recrystallised twice in methanol.

The compounds were identified by microanalysis and infrared spectroscopy, and also by mass spectroscopy in the case of $[Fe_5C(CO)_{15}]$.

TABLE 4

SELECTED BOND LENGTHS (Å) AND ANGLES (°) FOR $[N(PPh_3)_2][Fe_5N(CO)_{14}]$ (**2**)

Fe(1)–Fe(2)	2.611(3)	Fe(1)–C(11)	1.75(1)
Fe(1)–Fe(3)	2.585(2)	Fe(1)–C(12)	1.79(2)
Fe(1)–Fe(4)	2.579(3)	Fe(1)–C(13)	1.77(2)
Fe(1)–Fe(5)	2.564(4)	Fe(2)–C(21)	1.78(1)
Fe(2)–Fe(3)	2.599(3)	Fe(2)–C(22)	1.76(2)
Fe(2)–Fe(5)	2.646(3)	Fe(2)–C(23)	1.84(2)
Fe(3)–Fe(4)	2.550(3)	Fe(3)–C(31)	1.76(2)
Fe(4)–Fe(5)	2.629(3)	Fe(3)–C(32)	1.71(1)
		Fe(4)–C(41)	1.80(2)
Fe(1)–N	1.916(8)	Fe(4)–C(42)	1.80(2)
Fe(2)–N	1.84(1)	Fe(4)–C(43)	1.96(1)
Fe(3)–N	1.882(9)	Fe(5)–C(51)	1.75(2)
Fe(4)–N	1.83(1)	Fe(5)–C(52)	1.80(1)
Fe(5)–N	1.826(8)	Fe(5)–C(53)	1.80(2)
		Fe(3)–C(23)	2.56(3)
		Fe(3)–C(43)	2.05(2)
Fe(2)–C(23)–O(23)	164(2)		
Fe(4)–C(43)–O(43)	144(1)		
Other Fe–C–O 170–180			
max. e.s.d. 2			
mean 176			
N–P(1)	1.594(7)	P(1)–C(111)	1.780(8)
N–P(2)	1.557(8)	P(1)–C(121)	1.799(9)
		P(1)–C(131)	1.78(1)
		P(2)–C(211)	1.79(1)
		P(2)–C(221)	1.799(8)
		P(3)–C(231)	1.79(1)
P(1)–N–P(2)	144.2(8)		
N–P(1)–C(111)	110.9(4)	N–P(2)–C(211)	115.6(4)
N–P(1)–C(121)	107.6(4)	N–P(2)–C(221)	110.9(4)
N–P(1)–C(131)	114.3(5)	N–P(2)–C(231)	108.4(5)
C(111)–P(1)–C(121)	107.4(4)	C(211)–P(2)–C(221)	108.0(5)
C(111)–P(1)–C(131)	107.7(4)	C(211)–P(2)–C(231)	105.7(5)
C(121)–P(1)–C(131)	108.7(4)	C(221)–P(2)–C(231)	107.9(4)

Electrochemical studies

Cyclic voltammetry and polarography were performed with Tacussel apparatus comprising a Tacussel PRT 30-01 potentiostat, a GSATP generator and an XY recorder. The working electrode was a dropping-mercury electrode for the polarographic measurement and a carbon electrode for the cyclic voltammetry. Controlled potential electrolysis was performed with a Tacussel PRT 20-2 potentiostat and a IG4 integrator on mercury electrode. The background electrolyte was 0.1 *M* NBu_4BF_4. The reference electrode was a double junction SCE electrode and the auxiliary electrode a platinum wire.

X-ray study

Crystals were mounted for X-ray examination in argon filled capillary tubes. It

TABLE 5

SELECTED BOND LENGTHS (Å) AND ANGLES (°) FOR $[NBu_4]_2[Fe_5C(CO)_{14}]$ (3)

Fe(1)–Fe(2)	2.597(4)	Fe(1)–C(11)	1.74(2)
Fe(1)–Fe(3)	2.616(4)	Fe(1)–C(12)	1.78(2)
Fe(1)–Fe(4)	2.590(2)	Fe(1)–C(13)	1.74(2)
Fe(1)–Fe(5)	2.591(2)	Fe(2)–C(21)	1.72(2)
Fe(2)–Fe(3)	2.553(3)	Fe(2)–C(22)	1.80(1)
Fe(2)–Fe(5)	2.597(4)	Fe(2)–C(23)	2.15(2)
Fe(3)–Fe(4)	2.670(4)	Fe(2)–C(25)	2.28(2)
Fe(4)–Fe(5)	2.680(4)	Fe(3)–C(31)	1.81(2)
		Fe(3)–C(32)	1.75(2)
Fe(1)–C	2.00(1)	Fe(3)–C(23)	1.82(2)
Fe(2)–C	1.88(2)	Fe(4)–C(41)	1.75(2)
Fe(3)–C	1.84(2)	Fe(4)–C(42)	1.68(3)
Fe(4)–C	1.87(2)	Fe(4)–C(43)	1.80(2)
Fe(5)–C	1.87(2)	Fe(5)–C(51)	1.78(1)
		Fe(5)–C(52)	1.74(2)
		Fe(5)–C(25)	1.85(2)
Fe(3)–C(23)–O(23)	151(1)		
Fe(5)–C(25)–O(25)	154(2)		
Other Fe–C–O	173–178		
max. e.s.d.	2		
mean	177		
C–O	1.11–1.21		
max. e.s.d.	0.03		
mean	1.15		

	Cation I	Cation II
N–C	1.49–1.53	1.50–1.54
mean	1.51	1.52
max. e.s.d.	0.02	0.02
C–C	1.42–1.57	1.44–1.49
mean	1.50	1.47
max. e.s.d.	0.05	0.03
C–N–C	104–116	106–112
mean	109	109
max. e.s.d.	1	1
C–C–C	94–117	110–119
mean	110	115
max. e.s.d.	3	2

was not possible to measure their density. After survey photography by precession techniques, the selected crystal of each compound was set up on an automatic three circle diffractometer. In each case, cell dimensions and orientation matrices were obtained from the setting angles of 9 reflections in the range $15 < 2\theta < 30°$. The scintillation counter was fitted with a pulse-height analyser tuned to accept 90% of the Mo-K_α peak. A take-off angle of 2° was used.

Crystal data and data collection parameters are listed in Table 2. The intensities of the standard reflections were measured every 100 reflections; no significant variations were observed. If the counting rate exceeded 7000 counts s^{-1}, counting loss was taken into account. The data were corrected for Lorentz and polarisation effects but not for absorption. Complex neutral scattering factors [17] were used

TABLE 6

FRACTIONAL ATOMIC COORDINATES FOR **1** WITH e.s.d.'s IN PARENTHESES

Atom	*x/a*	*y/b*	*z/c*
Fe(1)	0.66781(5)	0.14889(8)	0.60903(2)
Fe(2)	0.67017(5)	0.30289(8)	0.67585(2)
Fe(3)	0.62441(5)	0.43447(8)	0.60255(2)
Fe(4)	0.50174(5)	0.22791(8)	0.57318(2)
Fe(5)	0.53867(5)	0.10887(8)	0.64945(2)
C	0.5790(3)	0.2740(5)	0.6261(2)
C(11)	0.7302(4)	0.2015(6)	0.5701(2)
O(11)	0.7706(4)	0.2194(6)	0.5457(2)
C(12)	0.7680(4)	0.0827(7)	0.6447(2)
O(12)	0.8319(4)	0.0288(8)	0.6649(2)
C(13)	0.6328(4)	−0.0259(6)	0.5869(2)
O(13)	0.6156(3)	−0.1398(5)	0.5737(2)
C(21)	0.6888(4)	0.1788(7)	0.7191(2)
O(21)	0.7076(4)	0.1105(7)	0.7486(2)
C(22)	0.7908(4)	0.3539(7)	0.6910(2)
O(22)	0.8659(3)	0.3762(7)	0.7015(2)
C(23)	0.6213(4)	0.4405(7)	0.7037(2)
O(23)	0.5871(4)	0.5222(7)	0.7206(2)
C(31)	0.6613(4)	0.5042(7)	0.5570(2)
O(31)	0.6867(4)	0.5516(7)	0.5302(2)
C(32)	0.5337(5)	0.5623(7)	0.6028(2)
O(32)	0.4769(4)	0.6395(6)	0.6044(2)
C(33)	0.7081(4)	0.5533(7)	0.6336(2)
O(33)	0.7557(4)	0.6428(6)	0.6488(2)
C(41)	0.3938(4)	0.3150(8)	0.5721(2)
O(41)	0.3260(4)	0.3703(8)	0.5718(2)
C(42)	0.5220(4)	0.3046(6)	0.5258(2)
O(42)	0.5290(4)	0.3410(6)	0.4937(1)
C(43)	0.4504(4)	0.0721(7)	0.5429(2)
O(43)	0.4162(4)	−0.0192(6)	0.5215(2)
C(51)	0.4753(4)	0.1831(7)	0.6853(2)
O(51)	0.4363(3)	0.2335(7)	0.7068(2)
C(52)	0.5892(5)	−0.0528(8)	0.6768(2)
O(52)	0.6197(6)	−0.1569(7)	0.6925(3)
C(53)	0.4433(4)	0.0065(7)	0.6215(2)
O(53)	0.3807(3)	−0.0668(6)	0.6088(2)

throughout all three structure solutions and refinements. All computations were performed on a CII IRIS 80 computer using the SHELX 76 system of programs [18].

In each structure solution, the Fe atom positions were determined from MULTAN and Patterson functions and the remaining non-hydrogen atoms from subsequent electron-density difference syntheses. The structures were refined by blocked matrix least squares. The phenyl groups of $[N(PPh_3)_2]^+$ were constrained to be regular hexagons (C–C 1.395 Å) and refined as rigid bodies. A C_2H_5 group of one of the $[NBu_4]^+$ groups was found to be partially disordered and was refined in two positions with occupation factors of 0.54 and 0.46. In each butyl chain of these cations, the C–C bond distances were constrained to be equal, with an e.s.d. of 0.03 Å. H atoms were positioned geometrically [C—H 1.08 Å and U 0.08 Å^2].

Reflections with $|F| < 3\sigma|F|$ were considered as unobserved and excluded from calculations. In the final stage of the refinement, a weighting scheme of the form

TABLE 7

FRACTIONAL ATOMIC COORDINATES FOR THE ANION **2** WITH e.s.d.'s IN PARENTHESES

Atom	x/a	y/b	z/c
Fe(1)	0.0376(1)	0.4756(1)	0.29546(9)
Fe(2)	0.1062(1)	0.5470(1)	0.42126(9)
Fe(3)	0.2138(1)	0.4750(1)	0.39065(9)
Fe(4)	0.1461(1)	0.5633(1)	0.27625(9)
Fe(5)	0.0306(1)	0.63546(9)	0.3004(1)
N	0.1265(6)	0.5619(5)	0.3491(5)
C(11)	−0.065(1)	0.4972(8)	0.212(1)
O(11)	−0.1342(9)	0.5072(7)	0.1548(8)
C(12)	0.0719(8)	0.3926(9)	0.2611(7)
O(12)	0.0883(7)	0.3389(7)	0.2353(6)
C(13)	−0.011(1)	0.4181(9)	0.334(1)
O(13)	−0.049(1)	0.3768(8)	0.3518(8)
C(21)	0.181(1)	0.623(1)	0.4859(9)
O(21)	0.2303(9)	0.6702(8)	0.5282(7)
C(22)	0.016(1)	0.560(1)	0.4334(8)
O(22)	−0.045(1)	0.5699(9)	0.4394(8)
C(23)	0.167(1)	0.457(1)	0.480(1)
O(23)	0.1951(9)	0.4083(7)	0.5237(7)
C(31)	0.2370(8)	0.367(1)	0.4048(6)
O(31)	0.2511(7)	0.2963(7)	0.4122(5)
C(32)	0.321(1)	0.5064(8)	0.4598(8)
O(32)	0.3962(8)	0.5280(7)	0.5078(6)
C(41)	0.1012(9)	0.5352(8)	0.1839(9)
O(41)	0.0700(8)	0.5176(7)	0.1259(6)
C(42)	0.213(1)	0.6531(9)	0.2836(7)
O(42)	0.2521(7)	0.7101(6)	0.2868(5)
C(43)	0.2480(9)	0.4829(8)	0.3163(6)
O(43)	0.3014(6)	0.4559(6)	0.3093(5)
C(51)	−0.076(1)	0.6502(7)	0.2886(8)
O(51)	−0.1483(9)	0.6590(7)	0.2800(8)
C(52)	0.084(1)	0.734(1)	0.3415(8)
O(52)	0.1208(8)	0.7951(7)	0.3665(6)
C(53)	−0.003(1)	0.6692(9)	0.212(1)
O(53)	−0.0343(9)	0.6949(7)	0.1552(7)

$w = 1/|\sigma^2(F)|$ was used. The agreement factors were defined as $R = \Sigma||F_{obs} - F_{calc}|/\Sigma F_{obs}$ and $R_w = \{\Sigma w(F_{obs} - F_{calc})^2/\Sigma w(F_{obs})^2\}^{1/2}$.

Selected bond lengths and angles are presented in Tables 3,4 and 5. The geometry and dimensions of the $[N(PPh_3)_2]^+$ and $[NBu_4]^+$ cations are similar to those in several other crystal structures. Larges U values for the terminal carbon atoms of the butyl chains revealed important thermal vibrations (or disorder) for these atoms. Fractional atomic coordinates for **1**, for the anion **2** and for the dianion **3** are presented in Tables 6,7 and 8. Lists of observed and calculated structure factors, thermal parameters, and full lists of atomic coordinates and bond lengths and bond angles are available from the authors.

TABLE 8

FRACTIONAL ATOMIC COORDINATES FOR THE DIANION **3** WITH e.s.d.'s IN PARENTHESES

Atom	x/a	y/b	z/c
Fe(1)	0.0756(1)	0.10476(9)	0.33858(9)
Fe(2)	0.1000(2)	0.16078(9)	0.2458(1)
Fe(3)	0.0819(2)	0.05729(9)	0.2327(1)
Fe(4)	−0.1306(2)	0.05855(9)	0.2300(1)
Fe(5)	−0.1086(2)	0.16724(9)	0.2406(1)
C	−0.026(1)	0.1103(6)	0.2269(5)
C(11)	0.025(1)	0.0633(7)	0.3823(8)
O(11)	0.003(1)	0.0366(6)	0.4178(6)
C(12)	0.108(1)	0.1646(7)	0.393(1)
O(12)	0.134(1)	0.2023(5)	0.4295(6)
C(13)	0.231(1)	0.0801(6)	0.3852(7)
O(13)	0.3384(9)	0.0669(5)	0.4219(5)
C(21)	0.093(1)	0.1903(7)	0.1718(8)
O(21)	0.0936(9)	0.2087(5)	0.1228(6)
C(22)	0.242(2)	0.1960(7)	0.3176(9)
O(22)	0.332(1)	0.2162(5)	0.3637(6)
C(23)	0.214(1)	0.0965(7)	0.2451(7)
O(23)	0.312(1)	0.0990(5)	0.2514(5)
C(25)	−0.024(1)	0.2291(7)	0.2422(7)
O(25)	−0.011(1)	0.2760(4)	0.2417(7)
C(31)	0.173(2)	−0.0039(7)	0.2785(8)
O(31)	0.228(1)	−0.0419(5)	0.3085(7)
C(32)	0.022(2)	0.0371(6)	0.141(1)
O(32)	−0.020(1)	0.0239(6)	0.0802(7)
C(41)	−0.087(2)	−0.0097(8)	0.2520(9)
O(41)	−0.062(1)	−0.0563(6)	0.2659(8)
C(42)	−0.0235(2)	0.0645(6)	0.254(1)
O(42)	−0.307(1)	0.0686(7)	0.2736(8)
C(43)	−0.249(1)	0.0487(6)	0.132(1)
O(43)	−0.328(1)	0.0437(6)	0.0718(6)
C(51)	−0.255(1)	0.1820(6)	0.1535(9)
O(51)	−0.350(1)	0.1903(5)	0.1009(6)
C(52)	−0.157(1)	0.1855(7)	0.2985(9)
O(52)	−0.193(1)	0.1972(6)	0.3355(6)

References

1 M. Boudart, Catal. Rev. Sci. Eng., 23 (1981) 1.
2 E.L. Muetterties and J. Stein, Chem. Rev., 79 (1979) 479.
3 S.D. Wijeyesekera, R. Hoffmann and C.N. Wilker, Organometallics, 3 (1984) 962.
4 B.F.G. Johnson, J. Lewis, W.J.H. Nelson, J.N. Nicholls, J. Puga, P.R. Raithby, M.J. Rosales, M. Shröder and M.D. Vargas, J. Chem. Soc., Dalton Trans., (1983) 2447.
5 B.F.G. Johnson, J. Lewis, J.N. Nicholls, J. Puga, P.R. Raithby, M.J. Rosales, M. Mc Partlin and W. Clegg, J. Chem. Soc., Dalton Trans., (1983) 277.
6 J.W. Kolis, F. Basolo and D.F. Shriver, J. Amer. Chem. Soc., 104 (1982) 5626.
7 B.A. Sosinsky, N. Norem and J. Shelly, Inorg. Chem., 21 (1982) 348.
8 I.A. Oxton, D.B. Powell, R.J. Goudsmith, B.F.G. Johnson, J. Lewis, W.J.H. Nelson, J.N. Nicholls, M.J. Rosales, M.D. Vargas and K.H. Whitmire, Inorganica Chimica Acta Letters, 64 (1982) L259.
9 R.P. Brint, K. O'Cuill, T.R. Spalding and F.A. Deeney, J. Organomet. Chem., 247 (1983) 61 and references therein.
10 R.P. Brint, M.P. Collins, T.R. Spalding and F.A. Deeney, J. Organomet. Chem., 258 (1983) C57.
11 (a) J.S. Bradley, Adv. Organomet. Chem., 22 (1983) 74; (b) J.S. Bradley, Phil. Trans. R. Soc. Lond., A308 (1982) 103.
12 R.E. Dessy, F.E. Stary, R.B. King and M. Waldrop, J. Amer. Chem. Soc., 88 (1966) 471.
13 E.H. Braye, L.F. Dahl, W. Hubel and D.L. Wampler, J. Amer. Chem. Soc., 84 (1962) 4633.
14 K. Wade, Adv. Inorg. Chem. Radiochem., 18 (1972) 99.
15 M. Tachikawa, R.L. Geerts and E.L. Muetterties, J. Organomet. Chem., 213 (1981) 11.
16 M. Tachikawa, J. Stein, E.L. Muetterties, R.G. Teller, M.A. Beno, E. Gebert, J.M. Williams, J. Amer. Chem. Soc., 102 (1980) 6648.
17 International Tables for X-ray Crystallography, 1974, Vol. IV, Birmingham, Kynoch Press.
18 Computer programs used were Sheldrick's SHELX 76, Johnson's ORTEP-2 and locally written routines.